Morphology and Mechanical Properties of Polyamide 12 Blends with Styrene/Ethylene–Butylene/Styrene Rubbers with and without Maleation

S. Jose,[1] S. Thomas,[1] E. Lievana,[2] J. Karger-Kocsis[2]

[1]*School of Chemical Sciences, Mahatma Gandhi University, Priyadarshini Hills P.O., Kottayam, Kerala, India 686 560*
[2]*Institute for Composite Materials, Kaiserslautern University of Technology, P.O. Box 3049, D-67653 Kaiserslautern, Germany*

Received 5 March 2004; accepted 2 September 2004
DOI 10.1002/app.21362
Published online in Wiley InterScience (www.interscience.wiley.com).

ABSTRACT: Blends of polyamide 12 (PA12) with styrene/ethylene–butylene/styrene (SEBS) and maleic anhydride grafted SEBS (SEBS-*g*-MA) were prepared by twin-screw extrusion and injection molding. The morphology, mechanical properties, and dynamic mechanical properties of the blends were studied. The morphology of the blends was evaluated from the etched surfaces of cryogenically fractured specimens with scanning electron microscopy. The morphological parameters showed that the PA12/SEBS-*g*-MA blends (PM series) exhibited a finer and more uniform rubber dispersion than the PA12/SEBS blends (PS series) because of the interfacial chemical reactions. SEBS functionalization via maleic anhydride grafting strongly affected the morphological parameters, such as the domain size, interfacial area per unit of volume, and critical interparticle distance, but the distribution of the rubber domains in the blends was less affected. Tensile and impact studies showed that the PS blends had worse mechanical properties than the PM blends. The tensile strength and elongation at break of the PM blends were considerably greater than those of the PS blends. The fracture toughness and energy values determined for notched Charpy specimens in high-speed impact tests were markedly higher for the PM blends than for the PS blends. A similar observation was obtained from instrumented falling weight impact studies. Dynamic mechanical analysis confirmed the incompatibility of the blend components because the glass-transition temperatures of PA12 and the rubber phase (SEBS and SEBS-*g*-MA) were not affected.
 J Appl Polym Sci 95: 1376–1387, 2005

Key words: blends; compatibilization; polyamides; structure-property relations; toughness

INTRODUCTION

Nowadays, reactive extrusion has been popularized as one of the most interesting techniques that can enhance the desired properties of polymer blends by interfacial chemical reactions between the blend components.[1] The block or graft copolymers formed by reactive extrusion reduce the interfacial tension (σ) and thus lead to a finer phase dispersion and better stability against coalescence. The concomitant improved interfacial adhesion promotes stress transfer between the blend constituents via the interface.[2]

Polyamides (PAs) are extensively used for engineering applications because of their good mechanical properties and excellent chemical and abrasion resistance. However, a significant deterioration of toughness at low temperatures prevents their more widespread use. It has been well demonstrated that the incorporation of functionalized rubbers based on ethylene–propylene–diene monomers, ethylene–propylene copolymer (EPR), styrene/ethylene–butylene/styrene block copolymer (SEBS), poly(ethylene–octene) elastomer (POE), and so forth into PAs improves their low-temperature toughness appreciably.[3–10] Oshishi et al.[3] investigated the effect of the end groups of PAs on the morphology generation and toughness of blends with maleated elastomers such as maleic anhydride (MA) functionalized SEBS and EPR (SEBS-*g*-MA and EPR-*g*-MA, respectively) and observed that the subambient toughness depended mainly on the inherent ductility of the PA matrix. Yu et al.[6] found that MA-grafted POE significantly improved the compatibility of POE with PA6 and prepared supertough blends. Kelnar et al.[8] reported that a combination of a styrene–MA copolymer with maleated EPR or SEBS with a total concentration of less than 15 wt % produced a ternary blend with PA6. The respective blend possessed a very high toughness in comparison with plain PA6, without the strength and stiffness being lowered.

Polyamide 12 (PA12), the lowest water-absorbing PA, shows excellent resistance toward solvents, abrasion, fatigue, and environmental stress cracking and

Correspondence to: J. Karger-Kocsis (jozsef.karger@ivw.uni-kl.de).

has good melt processability. SEBS is a triblock (ABA-type) thermoplastic elastomer that combines the melt processability of polystyrene (PS) and the elastomeric properties of poly(ethylene/butylene). SEBS and SEBS-*g*-MA are frequently used as impact modifiers and compatibilizers in polymer blends.[11–17] Kim et al.[12] studied the micromechanical deformation process in toughened polypropylene (PP)/PA/SEBS-*g*-MA blends and observed that the blend morphology, that is, the rubber dispersion, changed significantly with an increasing volume fraction of SEBS-*g*-MA. Bassani and coworkers[14,15,17] showed that the incorporation of SEBS-*g*-MA improved the impact strength of PP considerably.

Through the blending of PA12 with SEBS and SEBS-*g*-MA, we can produce supertough engineering thermoplastic elastomers with excellent processability and rubbery resilience. In contrast to PA6 and PA66 blends, less information is available on the toughening of PA12 blends. Therefore, it is challenging to develop supertough thermoplastics and thermoplastic elastomers with PA12. Lievana et al.[18] investigated the impact fracture and failure behavior of *in situ* polymerized ethylene/butyl acrylate rubber (E/BA) toughened PA12 and found that E/BA was an efficient toughness modifier when finely dispersed in PA12.

Because the toughness of blends depends on morphological characteristics (influenced by the rubber type and content, particle size and interparticle distance of the rubber, rubber particle cavitation behavior, etc.), it is important to study them as a function of the blend ratio in the presence and absence of reactive groups in the rubber modifier. In this article, we report on the morphology and mechanical properties of PA12 blends with SEBS and SEBS-*g*-MA rubbers. Characteristics of the rubber dispersion in the blends were determined with scanning electron microscopy (SEM) micrographs taken of etched fracture surfaces of the blends. Both static and dynamic mechanical properties were taken into account. Tensile and impact properties (high-speed flexural and perforation impact properties) of the blends were correlated with the morphological parameters. Finally, the extent of the property improvement of the blends with and without interfacial chemical reactions (primary and secondary amines with anhydride) was compared.

EXPERIMENTAL

Materials

PA12 (Vestamid L 1670), with a melt-volume-flow rate of 60 cm^3/10 min (at 250°C/2.16 kg) and a density of 1.01 g/cm^3, was kindly supplied by Degussa High Performance Polymers (Marl, Germany). SEBS (Kraton G-1652E), with a melt-flow index (MFI) of 1 dg/min (200°C/5 kg), and SEBS-*g*-MA (Kraton FG-1901X), with a 1.84 wt % MA graft ratio and an MFI of 20 dg/min (270°C/5 kg), were obtained from Shell Chemical Co. (Houston, TX). Both rubbers had a specific gravity of 0.91 g/cm^3, a styrene concentration of 30 wt %, and molecular weights of the PS and poly(ethylene-*co*-butene) copolymer blocks of approximately 7000 and 37,500 g/mol, respectively.

TABLE I
Compositions of the Blends and Their Codes

	PA12		SEBS		SEBS-*g*-MA	
System	wt%	vol%	wt%	vol%	wt%	vol%
PS5	95	95.5	5	4.5	—	—
PS10	90	90.9	10	9.1	—	—
PS20	80	81.8	20	18.2	—	—
PS50	50	54.5	50	45.5	—	—
PM5	95	95.5	—	—	5	4.5
PM10	90	90.9	—	—	10	9.1
PM20	80	81.8	—	—	20	18.2
PM50	50	54.5	—	—	50	45.5

Blend preparation

PA12 was dried in a vacuum oven at 80°C for 24 h before the blending. All the blends were prepared on a laboratory twin-screw extruder (length/diameter ratio = 22; DSE 25, Brabender, Duisburg, Germany) equipped with necessary accessories. The barrel temperatures were maintained at 180, 190, 200, and 220°C, and the rotor speed was optimized at 40 rpm. The extruded blends were pelletized with a homemade pelletizer. The extruded samples were dried again in a vacuum oven for 12 h before the injection molding. All the blends were injection-molded into dumbbell specimens 4 mm thick (according to ISO 3167) and film-gated plaques (80 mm × 80 mm) 1 mm thick in an injection-molding machine (320 S 500-150, Arburg, Lossburg, Germany). The mold and melting temperatures were maintained at 60 and 190–220°C, respectively. The compositions and codes of the blend systems are presented in Table I.

Morphology studies

The samples for the phase morphology studies were cryogenically fractured in liquid nitrogen. Each fractured surface was etched in toluene for 48 h for the extraction of the rubber phase. Each etched surface was sputter-coated with a Au/Pd alloy in a sputter-coating machine (SCD 050, Balzers, Liechtenstein) for 150 s. At least five photographs were taken for each sample with SEM (5400, JEOL, Tokyo, Japan). About 200 particles were considered for morphological parameter measurements. The number-average diameter (D_n), weight-average diameter (D_w), and volume-average diameter (D_v) were determined as follows:

$$D_n = \frac{\sum NiDi}{\sum Ni} \quad (1)$$

$$D_w = \frac{\sum NiDi^2}{\sum NiDi} \quad (2)$$

$$D_v = \frac{\sum NiDi^3}{\sum NiDi^2} \quad (3)$$

where Ni is the number of domains having diameter Di.

Mechanical property testing

Tensile testing

The tensile properties of the blends were determined at room temperature (RT) with a Zwick universal testing machine (model 1474, Zwick, Ulm, Germany) with an extensometer at a crosshead speed of 50 mm/min. Five dumbbell specimens were used for each blend to determine Young's modulus (E), the tensile strength (σ_b), and the elongation at break (ε_b).

High-speed flexural impact testing

Impact tests were performed on notched Charpy specimens. They were cut from the gauge sections of the injection-molded dumbbells.[19] The dimensions of the Charpy specimens were 80 mm (support length = 62 mm) × 10 mm × 4 mm. The specimens were notched with a Notchvis device from Ceast (Piannezza, Italy) for an a/W ratio of about 0.5, where W is the width and a is the notch length ($W - a$ is the free ligament of the specimens). The specimens were subjected to instrumented impact bending without the cushioning of the striker at RT. An instrumented impact pendulum from Ceast (DAS 8000) recorded the force during impact as a function of time. The primary data could be converted into other representation of the fractograms (force–deflection, energy–deflection, etc.) with the DAS 8 WIN (2.10) software of the device. The parameters of the impact tests were as follows: striker speed, 3.7 m/s; striker energy, 15 J; load range, up to 650 N; and sampling time, up to 8 ms. The fracture toughness (K_c) and fracture energy (G_c) were determined from the fractograms with the ESIS protocol[20] (ISO 17281) from five parallel tests.

High-speed perforation impact testing

The injection-molded plaques (80 mm × 80 mm) 1 mm thick were subjected to instrumented falling weight impact (IFWI) at RT. The plaques were clamped onto a supporting ring 40 mm in diameter and impacted with a dart 13 mm in diameter at an incident speed of 4 m/s. The incident energy of the dart was 25.7 J. Five specimens were used for each blend, and from the IFWI fractograms recorded by a Dartvis device from Ceast, the thickness (t)-related (specific) peak and perforation energy (E_{peak}/t and E_{perf}/t, respectively), the specific maximum load (F_{peak}/t), and the displacement at the maximum load (x_{peak}) were computed. The disc stress at the maximum load ($\sigma_{d,max}$) was calculated as follows:

$$\sigma_{d,max} = 2.5F_{max}/t^2 \quad (4)$$

There is a further parameter often used to characterize the fracture, that is, the ductility index. This parameter accounts for the relative energy dissipated in the postmaximum range until complete failure. This parameter was not considered because sheets of the PM series were fractured by stress (strain) hardening. During the related plastic deformation, the load increased significantly and became larger than the first peak (cf. related force–time fractograms later).

Dynamic mechanical thermal analysis

The dynamic mechanical properties of the blends were analyzed with a dynamic mechanical thermal analyzer (Eplexor 150 N, Gabo Qualimeter, Ahlden, Germany) in the tension mode. The static force and dynamic force were taken to be 10 and ± 5 N, respectively. Samples 4 mm thick and 10 mm wide were used. The dynamic frequency was kept constant at 10 Hz, and the heating rate was selected to be 1°C/min from −100 to +100°C.

RESULTS AND DISCUSSION

Morphology of the blends

The morphology of the cryogenically fractured and etched surfaces of both PS and PM blends can be evaluated from Figures 1(a–d) and 2(a–d), respectively. All the micrographs reveal a two-phase morphology due to the immiscible nature of the blends. A careful evaluation suggests that all the blends except PS50 had a particle droplet-type morphology, whereas the PS50 blend possessed a cocontinuous phase structure. The morphological parameters of all the blends derived from the micrographs are summarized in Table II. There was a large difference in the morphology characteristics of the two blend systems, that is, PS and PM.

Table II shows that the domain size of the dispersed rubber particles increased with increasing rubber concentration, as expected. A clearer picture is given in Figure 3, which compares the variations in the rubber

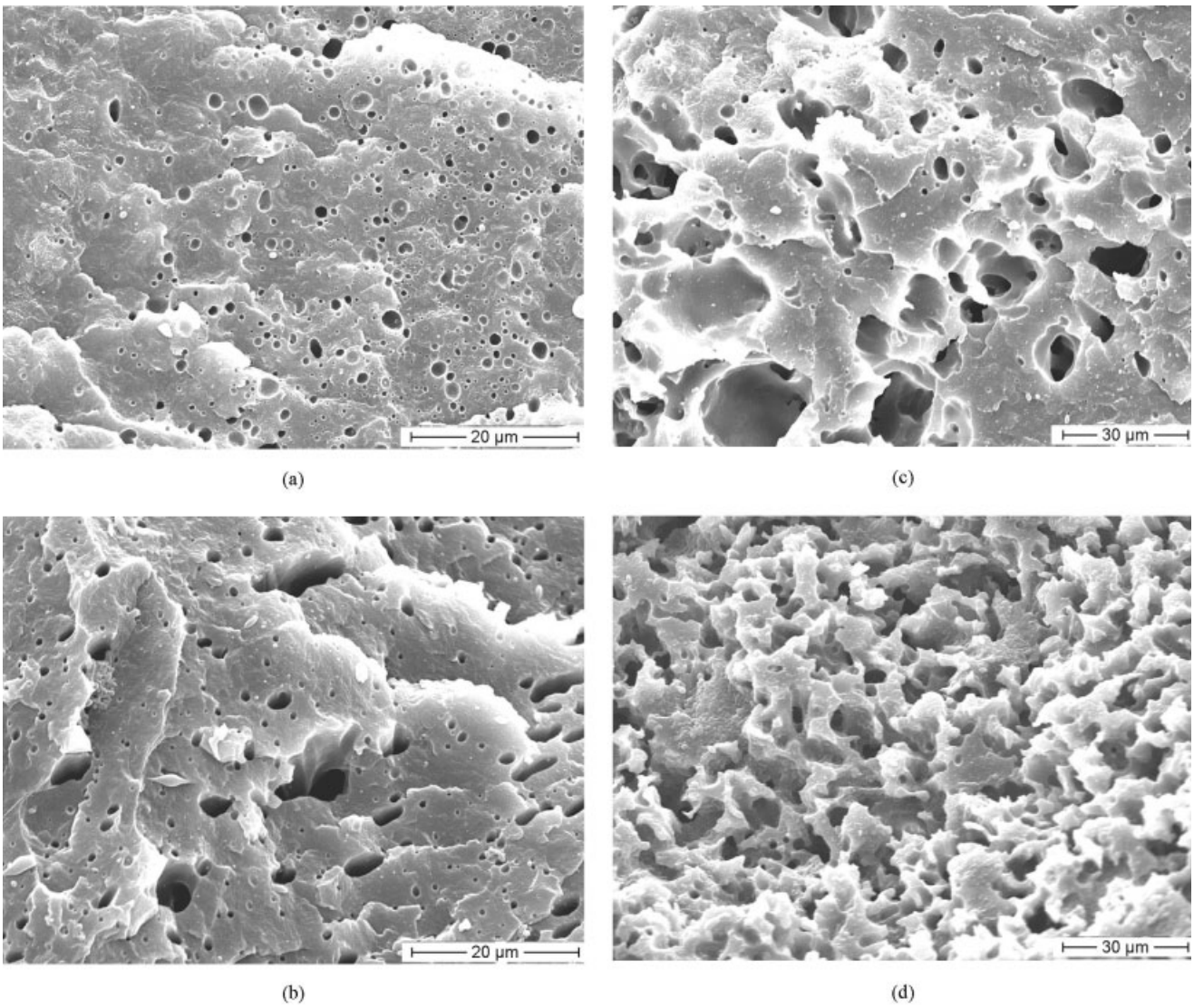

Figure 1 SEM pictures of cryogenically fractured etched surfaces of PS blends containing (a) 5, (b) 10, (c) 20, and (d) 50 wt % SEBS rubber.

domain size of the PS and PM blends as a function of the rubber concentration. It is well established that the final blend morphology is determined by the factors related to the material parameters (the blend composition, viscosity ratio, elasticity ratio, and σ) and processing conditions. More specifically, the final morphology is a balance between deformation and disintegration phenomena on the one hand and coalescence on the other hand. Taylor[21,22] studied the deformation and disintegration of the dispersed phase for Newtonian systems in simple shear-flow fields in the absence of coalescence effects. He defined a dimensionless parameter E:

$$E = C_a\{[(19p + 16)/(16p + 16)]\} \quad (5)$$

C_a, the capillary number, represents the ratio of viscous forces to interfacial forces:

$$C_a = \eta_m \dot{\gamma} R / \sigma \quad (6)$$

where η_m is the viscosity of the matrix, p is the viscosity ratio of the droplet phase to the matrix, R is the radius of the droplet, and $\dot{\gamma}$ is the shear rate. From Taylor equation, it is clear that the critical variables to consider in controlling particle deformation and breakup of the dispersed phase during the processing of polymer blends are p, $\dot{\gamma}$, the droplet diameter, and σ.

Tokita[23] derived an expression for the particle size of the dispersed phase in polymer blends that incorporates the composition as a variable. Tokita defined a rate constant for breaking the drops and one for coalescence. According to this theory, at equilibrium, when coalescence and breakdown are balanced, the

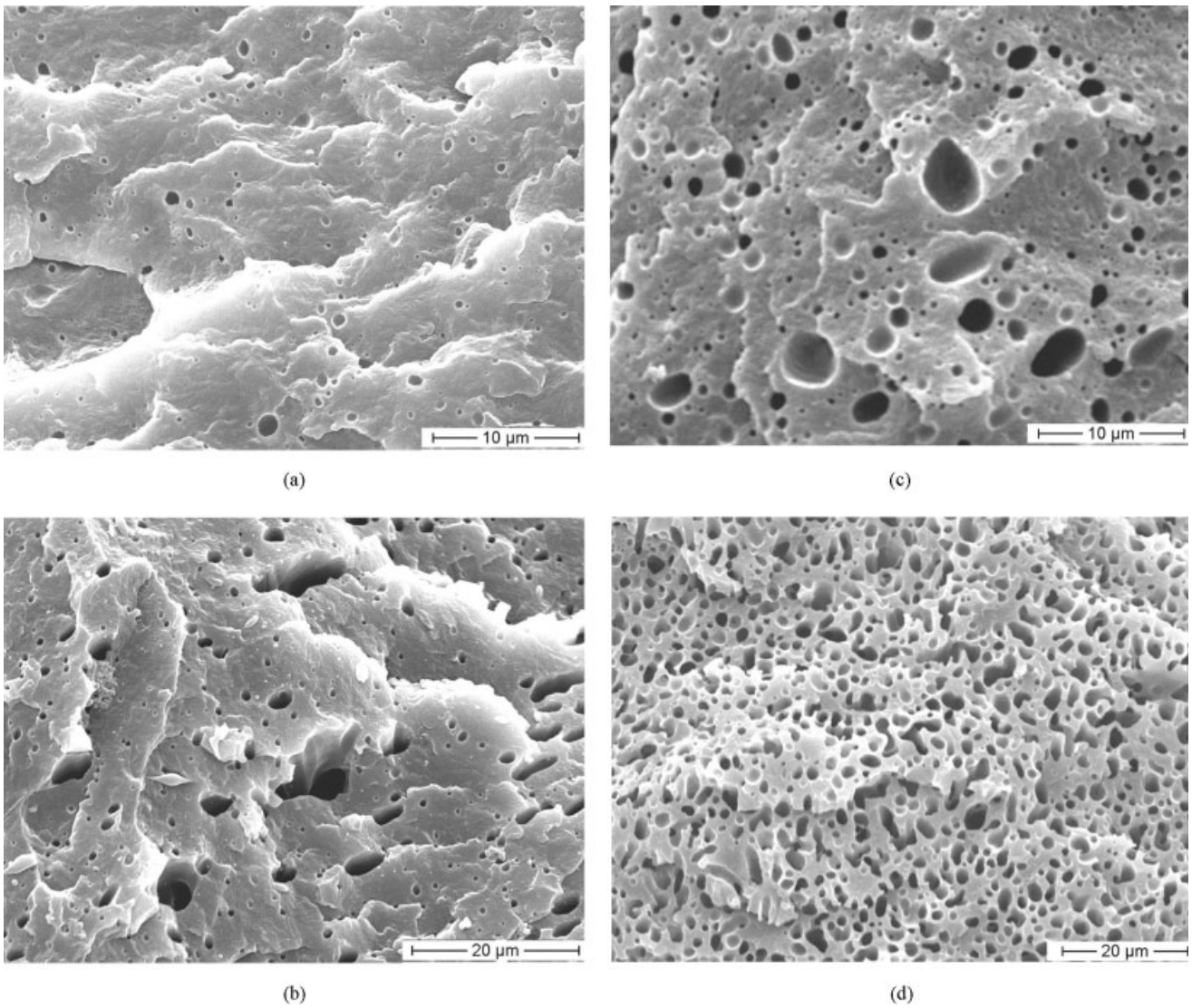

Figure 2 SEM pictures of cryogenically fractured etched surfaces of PM blends containing (a) 5, (b) 10, (c) 20, and (d) 50 wt % SEBS-*g*-MA rubber.

equilibrium particle size (d_e) can be obtained as follows:

$$d_e \cong 24P_r\sigma/\pi\tau_{12}[\phi_d + (4P_rE_{dk}/\pi\tau_{12})\phi_d^2] \quad (7)$$

TABLE II
Morphological Parameters of the PS and PM Blends

Blend	D_n (μm)	D_w (μm)	D_v (μm)	D_w/D_n	A_i ($\mu m^2/\mu m^3$)	IPDC (μm)
PS5	0.73	1.06	1.36	1.45	0.37	0.820
PS10	1.17	1.56	2.05	1.33	0.47	0.798
PS20	5.03	7.71	10.10	1.53	0.22	1.680
PM5	0.61	0.82	1.03	1.34	0.45	0.683
PM10	0.63	0.89	1.09	1.41	0.87	0.430
PM20	0.87	1.38	2.03	1.59	1.26	0.290
PM50	1.63	2.08	2.56	1.28	1.67	0.003

where τ_{12} is the shear stress, E_{dk} is the bulk breaking energy, ϕ_d is the volume fraction of the dispersed phase, and P_r is the probability that a collision will lead to coalescence.

From the Taylor equation, we can conclude that, increasing τ_{12} ($\tau_{12} = \eta_m\dot{\gamma}$) would result in a reduction in the droplet size, whereas the size of the dispersed droplet is directly related to σ between the two phases. However, other studies[24,25] have shown that the blend morphology is not sensitive to 2–3-fold changes in τ_{12} and $\dot{\gamma}$ in an internal mixer. At the same time, a direct experimental confirmation of the σ/particle-size relationship, as predicted by the Taylor theory, was demonstrated by Liang et al.[26] The authors showed that in the absence of coalescence effects, there is a close 1:1 relationship between the morphology and σ. Lepers et al.[27] studied the influence of the SEBS-*g*-MA compati-

bilizer on the relative role of coalescence suppression and σ reduction in PP/poly(ethylene terephthalate) blends. The authors showed that the particle size reduction was about equally due to σ and coalescence effects.

Tokita's theory predicted that the particle size at equilibrium would diminish as the magnitude of the stress field increased, σ decreased, and the volume fraction of the dispersed phase decreased. Thus, the extent of coalescence and the phase size versus the composition dependence depend to a large degree on σ of the immiscible pair. In PA12/SEBS blends, an increase in the dispersed particle size with an increase in the concentration of rubber is mainly attributable to (1) the increase in τ_{12} due to the enhancement in the viscosity of the system as the concentration of the rubber increases, (2) the increase in coalescence because as the concentration of the rubber phase increases the number of dispersed particles and therefore the probability of the particles colliding with each other increase, and (3) the increase in σ.

However, the increase in the domain size is much less for SEBS-*g*-MA than for SEBS (cf. the data for the PM and PS series in Table II). Figure 4 gives an idea about the increase in the domain size as a function of the rubber concentration in both systems. The domain size of 5 wt % rubber is taken as zero, and the increase in the domain size as a function of the rubber concentration is plotted. From 5 to 10 wt % rubber, the increase in the domain size of dispersed rubber in the PM blends is negligible, whereas in the PS blends, there is a considerable increase in the domain size (60%). Similarly, from 10 to 20 wt % rubber, the increase in the domain size for the PM blends is relatively small (40% increase from PM10 to PM20) compared to that for the PS blends (330% increase from PS10 to PS20). Also, the dispersed domain size in PM50 is smaller than that of PS20. All these factors show that there is a greater suppression of coalescence in PM blends than in PS blends. This is not unexpected and may be treated as direct evidence of the interfacial chemical reaction between PA12 and SEBS-*g*-MA (Fig. 1). If strong interactions are present at the interface, the average particle size can be independent of the composition right up to the region of dual-phase continuity. This has been well observed for the PA12/SEBS-*g*-MA blends, in which the formation of the compatibilizer at the interface drastically reduces σ. Thus, in the PA12/SEBS-*g*-MA system, interfacial modification appears to be dominant factor for controlling the dispersed phase size. Even the dependence of the phase size on the viscosity ratio is less pronounced.

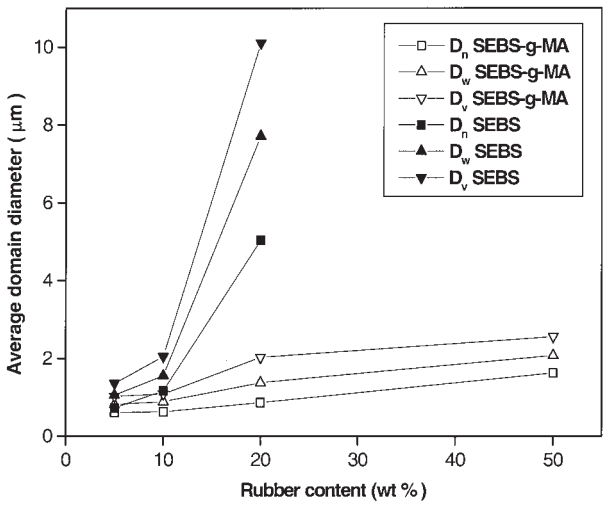

Figure 3 Variation in the rubber domain size (D_n, D_w, and D_v) for the PS and PM blends as a function of the rubber concentration.

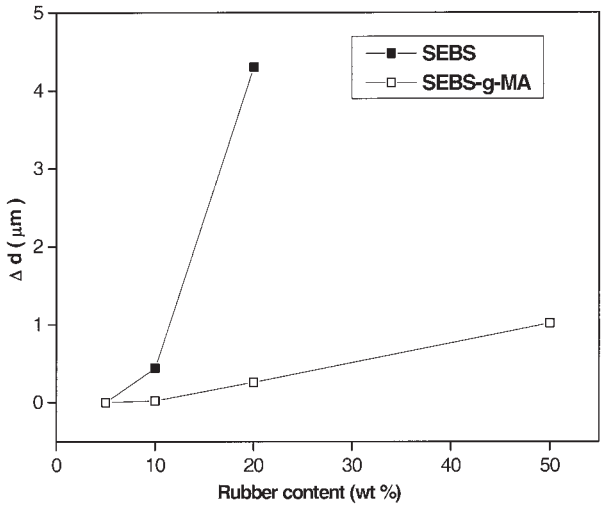

Figure 4 Relative change in the domain size (Δd) of the dispersed rubber in the PS and PM blends as a function of the rubber concentration.

With increasing concentration of the minor (dispersed) phase, the dispersed domain size also increases, and the interparticle distance becomes smaller. However, the chemical interactions between the matrix and dispersed phase restrict the diffusion merging of the dispersed particles. This can be easily understood by a comparison of SEM micrographs of PS50 and PM50 [Figs. 1(d) and 2(d), respectively]. PS50 possesses a well-developed cocontinuous phase structure, whereas PM50 retains a droplet-type structure even though the dispersed particles are very close to one another. The size distribution of the domains is less affected by increasing rubber concentration and by the chemical reactions, as shown by the polydispersity index (D_w/D_n) in Table II. The distributions of the rubber domains are depicted in Figure 5 for the PA12/SEBS and PA12/SEBS-*g*-MA blends.

The interfacial area (A_i) per unit of volume has been estimated with the following relationship:[2]

$$A_i = 3\phi/R \tag{8}$$

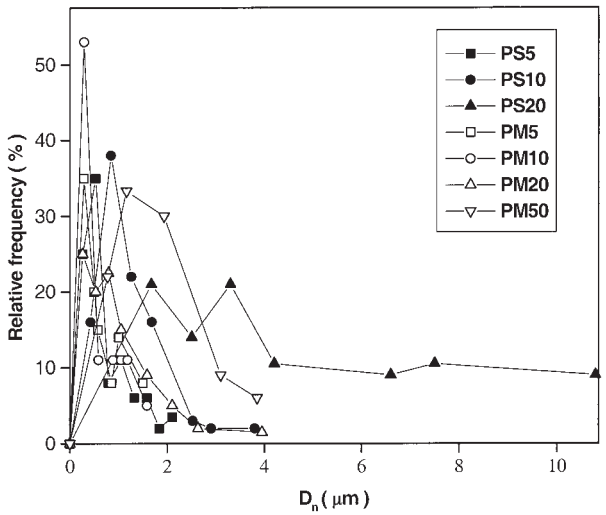

Figure 5 Size distribution of the rubber in the PS and PM blends as a function of the rubber concentration.

where ϕ is the volume fraction of the dispersed phase (cf. Table I) and R is the average radius of dispersed particles in a given blend (cf. Table II). The A_i values are presented in Table II. A_i increases gradually for the PM blends as the concentration of rubber in the blends is increased. On the other hand, for the PS blends, there is an increase in A_i from PS5 to PS10, and beyond that limit, a reverse tendency can be observed. However, when we compare the PS and PM blends, we can observe that A_i is significantly greater for PM blends. Furthermore, the relative increase in A_i with increasing rubber concentration is also greater for the PM blends than for the PS blends. A_i is a measure of interfacial thickness, which in turn is a measure of the compatibility of the blends. Thus, the PM blends are much more compatible than the PS blends. The latter exhibit a narrow interface that may fail because of stress transfer between the phases.

The critical interparticle distance (IPDC) has been calculated with Wu's equation:[28]

$$\text{IPDC} = D[(\pi/6\phi)^{1/3} - 1] \quad (9)$$

where D is the average domain diameter of the dispersed phase of volume fraction ϕ. The IPDC of PS blends is greater than that of corresponding PM blends. With increasing IPDC, the blend tends to fail brittlely upon mechanical loading. One can thus claim that PS blends are relatively more brittle than PM blends. For PS blends, IPDC slightly decreases just from PS5 to PS10, and beyond 10 wt % SEBS, there is tremendous increase in IPDC. This suggests that the related blends are prone to brittle failure. On the other hand, for PM blends, with increasing rubber concentration, IPDC decreases, and this suggests ductile failure behavior.

In short, the morphological parameters derived from micrographs of cryogenically fractured surfaces of blends show that PA12/SEBS-*g*-MA blends (PM series) exhibit a finer, more uniform, and more stable morphology than the PA12/SEBS blends (PS series). This is due to the interfacial chemical reactions. Thus, the PA12/SEBS-*g*-MA blends are more compatible and are expected to show higher ductility than the PA12/SEBS blends. Furthermore, it has been found that the MA functionality of rubber has a profound effect on morphological parameters such as the domain size, A_i, and IPDC. Interestingly, the distribution of the rubber domains (i.e., D_w/D_n) in the blends is less affected by maleation.

Mechanical properties of the blends

Tensile properties

Table III presents tensile properties such as E, σ_b, and ε_b of the PS and PM blends. Upon the addition of SEBS to PA12, E and σ_b decrease monotonically. On the other hand, ε_b increases with the addition of 5 wt % SEBS before a steep decline starts. Also, the ε_b values of the PS20 blend are unexpectedly low in comparison with those of the other blends.

A reduction in the tensile properties of the blends directly arises from the immiscibility of the blend components because of the lack of interactions at the interface. The result is high σ values and poor interfacial adhesion between PA12 and SEBS. This leads to a coarse morphology coupled with a poor stress-transfer possibility between the matrix and dispersed phase in the blend. Although σ_b shows a substantial decrease beyond even 5 wt % rubber in the blend, there is an abrupt reduction in E only beyond 20 wt % SEBS rubber in the blends. This is due to the fact that E, determined at low strains, depends less on the incompatibility than σ_b. Therefore, at a low rubber level, the decrease in E is due to the soft character (flexibility) of rubber rather than its incompatibility. On the other

TABLE III
Tensile Properties of the PA12 Blends with the SEBS and SEBS-*g*-MA Rubbers

Blend	E (MPa)	σ_b (MPa)	ε_b (%)
PA12	1495 ± 20	42 ± 1.2	327 ± 10
PS5	1376 ± 20	41 ± 1.2	371 ± 12
PS10	1202 ± 15	33 ± 0.8	242 ± 8
PS20	1040 ± 10	27 ± 0.8	24 ± 4
PS50	486 ± 10	14 ± 1	124 ± 2
PM5	1302 ± 12	45 ± 0.8	427 ± 14
PM10	1182 ± 10	45 ± 0.6	453 ± 10
PM20	976 ± 8	42 ± 0.5	489 ± 12
PM50	415 ± 10	>27	>500

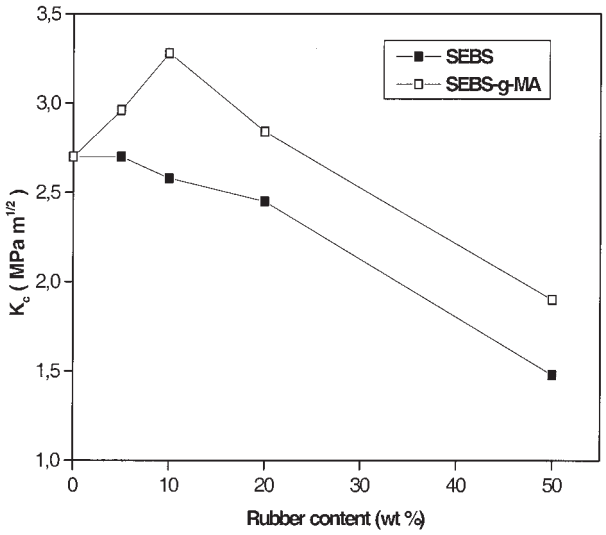

Figure 6 Variation of K_c as a function of the rubber concentration for the PS and PM blends.

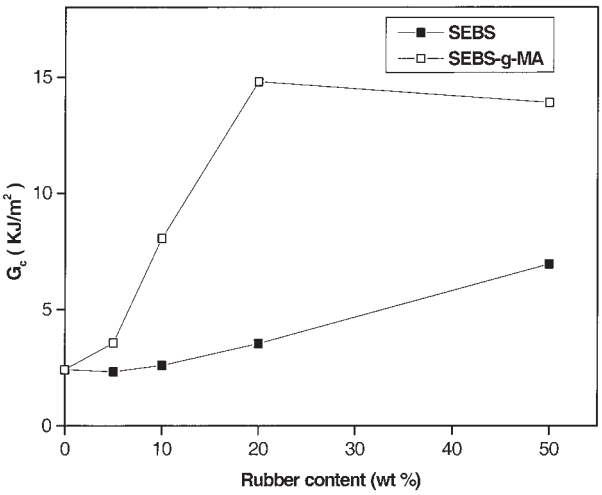

Figure 7 Variation of G_c as a function of the rubber concentration for the PS and PM blends.

hand, σ_b, determined at high strain levels, is highly dependent on the incompatibility of the blend components. As a result, E shows no substantial decrease even in the presence of 20 wt % SEBS because the major phase in the blend is still PA12. However, for a 50/50 blend in which both PA12 and SEBS form continuous phases, E is strongly reduced. σ_b sharply decreases even in the presence of 10 wt % SEBS in the blend. The reduction in σ_b can be directly linked to the morphological parameters. The unexpectedly low ε_b value of PS20 is due to the reduced A_i value and strongly enlarged IPDC (see Table II). Blends with 50 wt % SEBS show the minimum tensile mechanical properties, except for ε_b, because of the cocontinuous phase structure in these blends.

Table III shows that E of PM blends undergoes a gradual reduction with increasing rubber concentration in the blends. Similarly to PS blends, at a 50/50 blend ratio (PM50), there is a sharp reduction in E of the blends. On the other hand, σ_b of PA12 remains more or less constant upon the addition of even 20 wt % rubber. The PM20 blend possesses the same σ_b value as PA12, whereas it outperforms neat PA12 in terms of ε_b (50% increase in ε_b). However, for the PM50 blends, σ_b could not be measured exactly because the samples did not break up to 500% elongation, which is the maximum limit of the Zwick 1474 universal testing machine. ε_b increases steadily with increasing SEBS-*g*-MA in the blends. Adding only 5 wt % SEBS-*g*-MA to PA12 results in a considerable increase in the ductility.

High-speed flexural impact properties

K_c decreases for PS but goes through a maximum for the PM blends as a function of the rubber content (Fig. 6). K_c is a force (stress)-linked fracture mechanical parameter. We thus expect in the first approximation that a similar tendency can be observed for K_c as for σ_b as a function of the rubber loading. This prediction holds in our case, at least for the PS series (cf. data in Fig. 6 and Table III). However, strength-related parameters from high-speed flexural tests (dynamic) and from low-speed tensile ones (static) do not necessarily correlate with one another.

For toughened polymers, the G_c data are more relevant than K_c. Figure 7 shows that SEBS is a far less efficient modifier than SEBS-*g*-MA. The large difference in G_c between the PS and PM series can be traced to alterations in the morphological parameters listed in Table II. High G_c values in very tough rubber-modified thermoplastics are usually due to a plane-

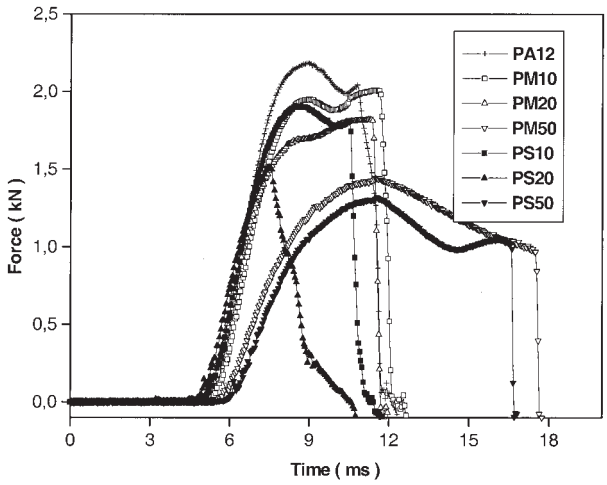

Figure 8 Typical perforation impact fractograms (force–time traces) as a function of the rubber concentration for the PS and PM blends.

TABLE IV
High-Speed Perforation Impact Properties of the PS and PM Blends

Blend	F_{max}/t (kN/mm)	E_{peak}/t (J/mm)	E_{perf}/t (J/mm)	x_{peak} (mm)	$\sigma_{d,\,max}$ (GPa)
PA12	2.17	15.7	23.4	10.8	5.4
PS5	1.94	13.7	23.0	11.9	4.8
PS10	1.91	13.8	21.0	11.0	4.7
PS20	1.53	8.2	13.0	8.5	3.8
PS50	1.31	15.0	24.0	18.6	3.3
PM5	2.09	14.6	23.9	11.4	5.2
PM10	1.99	22.4	23.2	11.7	5.0
PM20	1.82	20.2	21.7	11.9	4.5
PM50	1.44	17.7	24.2	16.7	3.6

The scatter range of the data is within ± 5%.

strain/plane-stress transition triggered by the fine dispersion of the rubber. Under plane-stress conditions, the energy absorption is markedly larger than under plane strain because after cavitation of the rubber particles in the former case, considerable matrix deformation (yielding, shear flow, and crazing) may occur. The difference in G_c between the PS and PM blends becomes obvious when one looks at the broken notched Charpy specimens. The size of the stress-whitened zone near the fracture plane was very prominent in the PM blends compared with that in the PS blends. Stress whitening is caused by rubber cavitation, after which plastic deformation of the PA12 matrix takes place.

Perforation impact properties

Characteristic fractograms (force–time traces) registered during the perforation (instrumented falling weight) impact of PS and PM sheets are depicted in Figure 8, and the related deduced data are summarized in Table IV. Adding SEBS and SEBS-*g*-MA reduces the terms related to the specific disk stiffness (F_{max}/t) and disc stress (σ_d) because of the weakening effect of the rubber in the blends. Rubber particles act as stress concentrators, promote yielding in the interparticle ligaments, and thus lower the yield stress of the blends. This finding is again in agreement with the static mechanical data (cf. the related data in Tables III and IV). Thus, the falling dart impact results suggest that the same mechanisms are at work for the out-of-plane loading of the sheets. The ductility, reflected by the fracture time in Figure 8 of the PM blends containing more than 5 wt % rubber, is higher than that of PA12. Interestingly, the difference in the ductility between the PM and PS blends is much smaller than expected. This is due to the biaxial-type loading of the disks that happens in this test. In some cases, the large difference between the PS and PM blends is still there (see the related fractograms of PS20 and PM20 in Fig. 8 and the corresponding data in Table IV). The thickness-related (specific) perforation impact energy (E_{perf}/t) is a combined term as the effects of the loadability and ductility of the blend discs are involved there. Data in Table IV show that E_{perf}/t values practically do not change with the SEBS-*g*-MA content. On the other hand, E_{perf}/t goes through a minimum (at 20 wt %) for the PS series containing nonmaleated rubber. The basic difference in the failure mode between the PS and PM series is shown in Figure 9 for the 20 wt % rubber containing blends. The final failure of PS20 was introduced by stress whitening [cf. Fig. 9(a)], but without accompanying plastic deformation as registered by PM20 [cf. Fig. 9(b)]. This plastic yielding just along the circumference of the dart is the rationale behind the stress hardening observed in the related fractograms in Figure 8. The reason behind the consistency of the perforation energy values with the type of rubber (except for PS20) is the related failure mechanisms. PM blends fail by localized yielding (i.e.,

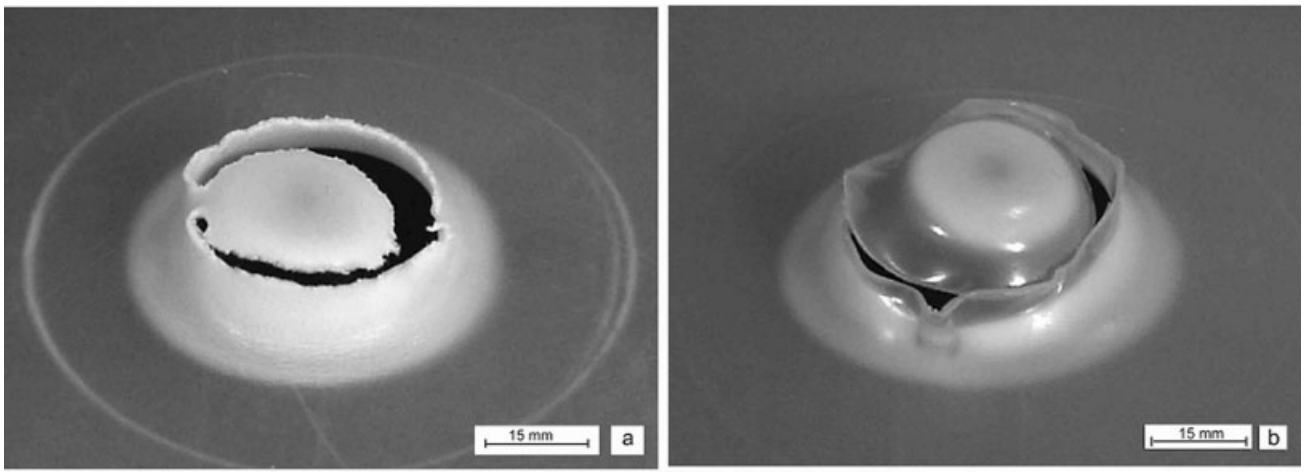

Figure 9 Macrophotographs (bottom view) of perforated sheets of (a) PS20 and (b) PM20.

TABLE V
Comparison of the Morphological and Mechanical Properties of the PS and PM Blends

Rubber (wt %)	Difference between the PM and PS blends						
	Morphology (%)			Mechanical properties (%)			
	D_n	A_i	IPDC	σ_b	ε_b	G_c	E_{perf}/t
5	20	22	20	10	15	60	3
10	85	85	86	46	87	150	10
20	480	473	480	56	>1900	376	67

along the circumference of the dart), whereas the corresponding PS blends produce massive and more extended crazing. The overall energy dissipation in the two cases is practically the same. There is no correlation between the E_{perf}/t and G_c data (cf. corresponding values in Tables III and IV).

In summary, it is obvious from the results that the PA12/SEBS-*g*-MA blends outperform the PA12/SEBS blends in terms of mechanical properties. There is an unparalleled correlation between the morphological parameters and mechanical properties. Table V demonstrates how intimately the mechanical properties are linked to the morphology of the blends and, at the same time, how intensely both the PS and PM blends differ in terms of the morphology and mechanical properties. With just 5 wt % rubber, the PS and PM blends show significant differences in the morphological parameters and, therefore, mechanical properties. The difference in the morphological parameters between PS5 and PM5 is 20%, and there are 10 and 15% differences between the two blends for σ_b and ε_b, respectively. There is a relatively large difference in G_c (60%) between the two blends, whereas E_{perf}/t shows the smallest difference (3%). On the other hand, the differences between PS10 and PM10 in the morphology and mechanical properties are markedly larger. There is more than an 80% difference between the PS and PM blends in the morphological parameters. The difference in σ_b is 46%, whereas ε_b shows almost the same difference as the morphological parameters. Among the different mechanical properties, G_c registers the maximum difference, whereas E_{perf}/t shows the minimum. The latter test represents a special kind of biaxial loading. The difference between the blends, in terms of the morphology, becomes maximum (≅480) when the rubber concentration reaches 20 wt %. The PS and PM blends register the maximum dif-

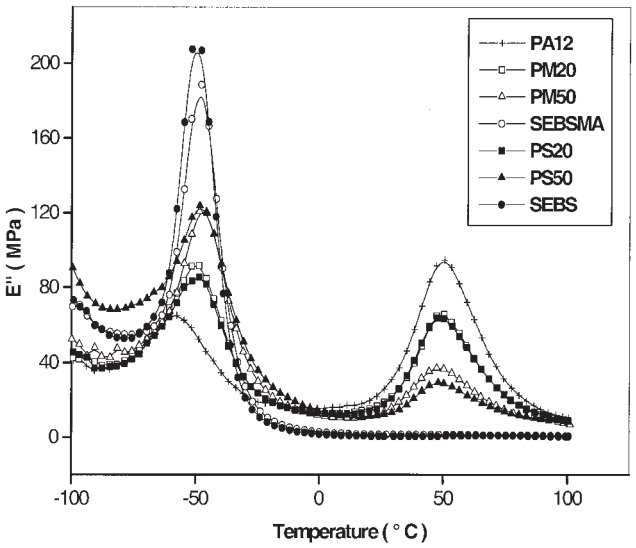

Figure 11 Dependence of E'' on the temperature for the PS and PM blends.

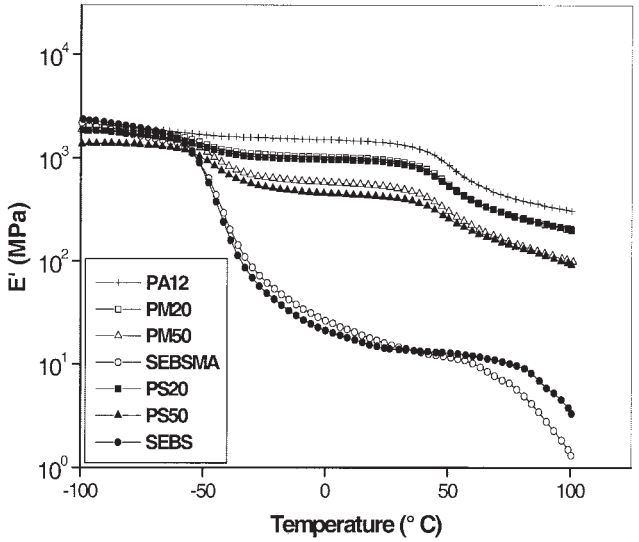

Figure 10 Dependence of E' on the temperature for the PS and PM blends.

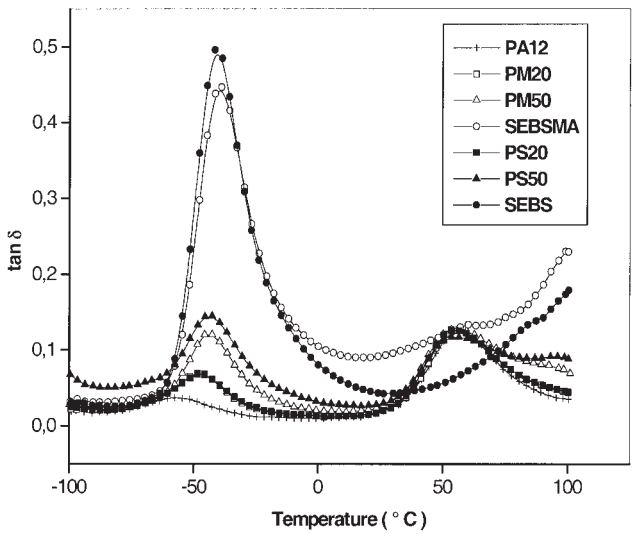

Figure 12 Dependence of tan δ on the temperature for the PS and PM blends.

TABLE VI
T_g of PA12, SEBS, and SEBS-*g*-MA in Their Virgin Forms and in the Related Blends

Blend	T_g from E'' vs Temperature (°C)			T_g from tan δ vs Temperature (°C)		
	PA12	SEBS	SEBS-*g*-MA	PA12	SEBS	SEBS-*g*-MA
PA12	50, −58[a]	—	—	56, −57[a]	—	—
SEBS	—	−49	—	—	−41	—
SEBS-*g*-MA	—	—	−47	—	—	−40
PS20	50	−49	—	56	−47	—
PS50	50	−48	—	55	−43	—
PM20	49	—	−49	53	—	−47
PM50	47	—	−45	53	—	−43

[a] Secondary relaxation of PA12.

ference in the mechanical properties at this composition, too. σ_b shows a 56% difference, whereas ε_b surprisingly shows a huge difference (more than 20 times than that between PS20 and PM20). There is an enormous difference in G_c (more than two times between PS20 and PM20), but the difference is much less in E_{perf}/t (ca. 60% between PS20 and PM20). Thus, in general, one can claim that there is an enormous difference in the morphological parameters between PS (without maleation) and PM (with maleation) blends, and this is well reflected in their mechanical properties. Thus, it can be concluded that both the morphology and mechanical properties of PA12/SEBS and PA12/SEBS-*g*-MA blends are intimately related.

Dynamic mechanical properties of the blends

Figure 10 presents the storage moduli (E') of PA12, SEBS, and SEBS-*g*-MA and their blends as a function of the temperature. E' of PA12 considerably decreases with the addition of rubber to the blend. This agrees with the courses of σ_b and E. Furthermore, we can observe the effect of MA functional groups: PA12/SEBS-*g*-MA blends possess greater storage modulus (E') than PA12/SEBS blends, and the difference is more pronounced for the blends with 50 wt % rubber. However, at higher temperatures (>50°C), this difference disappears.

The loss moduli (E'') and loss factor (tan δ) of PA12, SEBS, and SEBS-*g*-MA and their blends as a function of the temperature are given in Figures 11 and 12, respectively. The glass-transition temperature (T_g) of PA12, SEBS, and SEBS-*g*-MA in their virgin forms and in the blends derived from Figures 11 and 12 are listed in Table VI. T_g of virgin PA12 can be observed around 50°C, and a peak corresponding to a secondary relaxation of PA12 can be observed around −57°C. The T_g values of SEBS and SEBS-*g*-MA are −49 and −47°C, respectively. Furthermore, a part of the relaxation peak close to 100°C can be assigned to the PS blocks in both SEBS and SEBS-*g*-MA rubbers. All the blends show two peaks corresponding to the T_g's of both PA12 and rubber phases. This reveals the immiscibility of the blend components and agrees with the morphology found. Blending has no appreciable effect on the T_g's of PA12, SEBS, and SEBS-*g*-MA. Interestingly, the peak corresponding to the PS block cannot be resolved in the blends. From the morphological data and mechanical behavior, we can predict a shift in T_g of the PA phase in the PM blends because of the better compatibility achieved by interfacial chemical reactions. Unfortunately, it is not seen in reality. At the same time, the peak corresponding to the secondary relaxation of PA12 can hardly be located in the blends.

CONCLUSIONS

From this study, which is devoted to the investigation of the morphology and mechanical properties of PA12 blends with SEBS and SEBS-*g*-MA, the following conclusions can be drawn:

1. PA12/SEBS-*g*-MA blends exhibit a finer and more uniform rubber dispersion than PA12/SEBS blends because of the lack of interfacial chemical reactions in the latter case. The MA functionality of rubber plays a prominent role in determining the morphology of the blends.
2. The mechanical properties of PA12/SEBS-*g*-MA blends are superior to those of PA12/SEBS blends. ε_b tremendously increases upon the addition of SEBS-*g*-MA to PA12, whereas σ_b remains more or less unaffected up to a 20 wt % rubber concentration. There is an enormous difference in G_c in the presence and absence of maleated SEBS. SEBS-*g*-MA is therefore a highly suitable impact modifier for PA12. The mechanical properties of the blends are intimately related to the morphological parameters.
3. E' of PA12 decreases upon blending with rubber, whereas blending has no effect on T_g of the individual blend components.

References

1. Groeninckx, G.; Thomas, S.; Harrats, C. In Reactive Polymer Blending; Baker, W. E.; Scott, C.; Hua, G. H., Eds.; Hanser: Munich, 2001; p 43.

2. Thomas, S.; Groeninckx, G. Polymer 1999, 40, 5799.
3. Oshishi, A. J.; Keskkula, H.; Paul, D. R. Polymer 1992, 33, 284.
4. Burgisi, G.; Paternoster, M.; Peduto, N.; Saraceno, A. J Appl Polym Sci 1997, 66, 777.
5. Huang, D. D.; Wood, B. A.; Flexman, E. A. Adv Mater 1998, 10, 1207.
6. Yu, Z.; Ou, Y.; Hu, G. J Appl Polym Sci 1998, 69, 1711.
7. Tjong, S. C.; Xu, Y.; Meng, Y. Z. J Appl Polym Sci 1999, 72, 164.
8. Kelnar, I.; Stephan, M.; Jakisch, L.; Fortelny, I. J Appl Polym Sci 1999, 74, 1404.
9. Chen, H.; Yang, B.; Zang, H. J Appl Polym Sci 2000, 77, 928.
10. Karayannidis, G. P.; Bikiaris, D. N.; Papageorgiou, G. Z.; Bakirtzis, V. Adv Polym Technol 2002, 21, 153.
11. Tjong, S. C.; Xu, S. A. J Appl Polym Sci 1998, 68, 1099.
12. Kim, G. M.; Michler, G. H.; Rösch, J.; Mülhaupt, R. Acta Polym 1998, 49, 88.
13. Xu, S. A.; Tjong, S. C. J Appl Polym Sci 2000, 77, 2024.
14. Bassani, A.; Pessan, L. A.; Hage, E. J Appl Polym Sci 2001, 82, 2185.
15. Bassani, A.; Pessan, L. A. J Appl Polym Sci 2002, 86, 3466.
16. Tjong, S. C.; Xu, S. A.; Mai, Y. W. J Polym Sci Part B: Polym Phys 2002, 40, 1881.
17. Bassani, A.; Pessan, L. A. J Appl Polym Sci 2003, 88, 1081.
18. Lievana, E.; Wollny, A.; Mülhaupt, R.; Karger-Kocsis, J. Macromol Mater Eng 2002, 287, 266.
19. Karger-Kocsis, J.; Varga, J.; Ehrenstein, G. W. J Appl Polym Sci 1997, 64, 2057.
20. Pavan, A. In Fracture Mechanics Testing Methods for Polymers, Adhesives and Composites; ESIS Publication 28; Moore, D. R.; Pavan, A.; Williams, J. G., Eds.; Elsevier: Oxford, 2001; p 27.
21. Taylor, G. T. Proc R Soc London Ser A 1932, 138, 41.
22. Taylor, G. T. Proc R Soc London Ser A 1934, 146, 501.
23. Tokita, N. Rubber Chem Technol 1977, 50, 292.
24. Favis, B. D. J Appl Polym Sci 1990, 39, 285.
25. Favis, B. D. Makromol Chem Macromol Symp 1992, 56, 143.
26. Liang, H.; Favis, B. D.; Yu, Y. S.; Eisenberg, A. Macromolecules 1999, 32, 1637.
27. Lepers, J. C.; Favis, B. D.; Lacroix, C. J Polym Sci Part B: Polym Phys 1999, 37, 939.
28. Wu, S. Polymer 1985, 26, 1855.